Estimation of Individual Tree Health Condition for Japanese Mountain Cherry (*Cerasus jamasakura*) Using Airborne LiDAR

Takeshi Sasaki, Junichi Imanishi, Yoshihiko Iida, Youngkeun Song, Yukihiro Morimoto, and Tamao Kojima

Abstract. This study examined the usefulness of airborne light detection and ranging (LiDAR) data for estimating the individual tree health condition in Japanese mountain cherry (*Cerasus jamasakura*) in Yoshinoyama, Nara Prefecture, Japan. LiDAR variables that represented the ratio of lasers hitting tree components were calculated and their effectiveness was examined by relating them to the results of conventional field-based visual tree health assessments based on ordination, correlation analyses, and generalized linear models. The results showed that many of the LiDAR variables had significant correlations with the variables derived from visually evaluated tree health condition. In particular, the proportion of "only" returns, which represents the ratio of the lasers reflected from the crown surfaces, was the most effective for estimating total health condition in relation to the crown density, one of the key health indicators for representing physical properties. The individuals with large estimation errors had smaller crowns than the individuals with small errors, suggesting that sufficiently large crown sizes are important for more accurate estimations of the tree health condition using airborne LiDAR data.

Key Words. Airborne Laser Scanning; Detrended Correspondence Analysis; Hemispherical Photography; Single Tree Level; Tree Crown Density; Tree Health Assessment.

INTRODUCTION

Tree health condition is one of the most important parameters for monitoring and proper management of trees and forests which provide various ecosystem services (Ferretti 1997; Nielsen et al. 2014). Evaluation procedures of the tree crown health based on visual observations have been developed at the individual tree level, which are provided by the United States Department of Agriculture (Schomaker et al. 2007). Many studies have also evaluated the condition of crowns using visual procedures (Long et al. 1997; Schaberg et al. 2006; Scowcroft et al. 2007; Pontius and Hallett 2014). Similarly, in Japan a visual tree health evaluation method based on several indicators, including the tree form, crown dieback, and crown density, is used widely (Hasegawa et al. 1984; Kozawa and Kobayashi 1999; Imanishi et al. 2011; Iida et al. 2013). These visual methods are often subjective and differences between the evaluations made

by observers have been reported (Mizoue and Dobbertin 2003; Nakajima et al. 2011). Passive optical remote sensing data from satellites or aerial images can provide an objective evaluation of tree condition for a large area by calculating vegetation indices, such as the normalized difference vegetation index, although the estimation accuracies are lower than visual assessments (Michez et al. 2016). The passive optical sensors cannot penetrate canopies and therefore fail to acquire precise 3-D (three-dimensional) information, and many of the vegetation indices become saturated at high levels of leaf densities (Chen and Cihlar 1996; Sasaki et al. 2016b).

Light detection and ranging (LiDAR) is an active remote sensing technology which can directly acquire 3-D structure information (Lefsky et al. 2002; Griffith et al. 2015; Sasaki et al. 2016a). The LiDAR system emits numerous laser pulses (tens of thousands of pulses per second) and records one or more discrete

returns or a continuous waveform for each laser emission (Lim et al., 2003). LiDAR is less susceptible to weather conditions compared to optical sensors and it is effective for measuring objects with complex 3-D structures such as trees and forests (Wulder et al. 2008). Information about the objects hit by the lasers is converted into a large number of point cloud data, which all have x-, y-, and z-coordinate values, as well as attributes such as the intensity and return number. At the forest stand level, the canopy coverage and porosity have been estimated with high accuracies using variables based on the laser canopy hits and laser penetration rate derived from LiDAR data (Sasaki et al. 2008; Hopkinson and Chasmer 2009; Korhonen et al. 2011; Sasaki et al. 2016b). Thus, physical properties of trees such as their crown density and porosity may be estimated by applying these estimation methods at the individual tree level. Furthermore, the health condition of a tree can be estimated if it correlates with these physical indicators. Although many past studies identified individual trees in forests and estimated tree characteristics using LiDAR data (Popescu et al. 2003; Holmgren et al. 2008; Ørka et al. 2009), relatively few studies monitored trees outside forests (Schell et al. 2015), and none have associated the LiDAR variables with field-based visual tree health evaluations.

In this study, we aimed to verify the effectiveness of using airborne LiDAR data for estimating the individual tree health condition of Japanese mountain cherry (*Cerasus jamasakura*) planted in Yoshinoyama, Japan. In particular, we focused on the crown density, which is a visual health indicator, and used the crown porosity data obtained from hemispherical photographs to support the objectivity of the visual health assessment.

METHODS

Study Site
Yoshinoyama (34° 22' N, 135° 52' E), located in Nara Prefecture, Japan, is known for its cultural landscape containing flowering cherry trees. It has been designated as a UNESCO World Heritage Site because of the Sacred Sites and Pilgrimage Routes in the Kii Mountain Range. It has an elevation range of ca. 200 to 850 m above sea level, where cherry trees (mostly Japanese mountain cherry [*Cerasus jamasakura*]) have traditionally been planted for about 1,300 years (Imanishi et al. 2016). At present, the total planted

area is about 50 hectares (0.5 km²). The four main planted areas are known as Shimosenbon, Nakasenbon, Kamisenbon, and Okusenbon, in order from the lowest elevation (Figure 1). Recently, local residents have become concerned about declined tree health condition, which is inferred to be caused by multiple factors, including soil water retention ability determined by the topography, infection of fungus, and barkfeeding damage by animals (Imanishi et al. 2012).

Field Survey
We selected 11 clusters comprising a total of 324 cherry trees (Figure 1). We aimed to include trees in various health conditions throughout the entire area of Yoshinoyama. In August 2011, each tree was visually classified by two experts according to one of four health ranks (1 = good to 4 = poor) taking into account the following eight indicators: tree vigor, tree form, branch growth, crown dieback, crown density, leaf shape and size, leaf color, and bark condition, in accordance with the Japanese traditional method (Shibata 2007; Table 1).

For each tree, the stem location was measured using differential GPS and total station; the crown projection area was depicted using total station by finding the apexes of branches and connecting them. Each crown projection area on the ground was transformed into a polygon with ArcGIS and its area was calculated. We excluded five trees with excessively small crowns that did not produce any meshes when
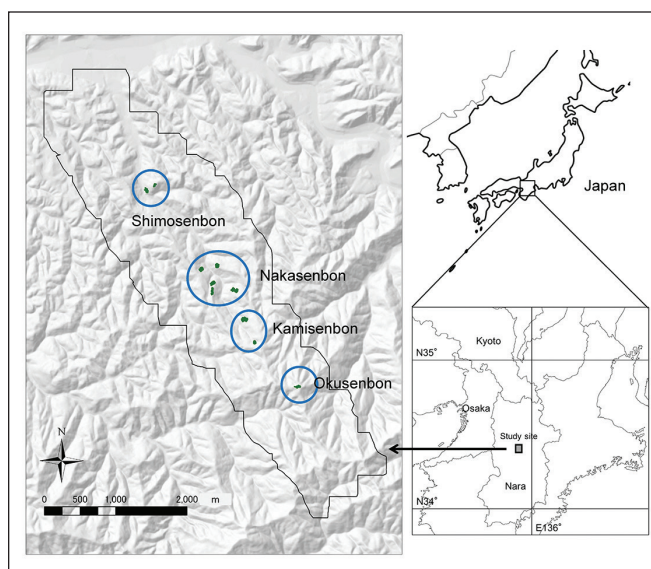

Figure 1. Location of the study site and distribution of *C. jamasakura* trees tested in the present study. The black border and dots represent the LiDAR data collection area and tested trees, respectively.

the polygons were converted into 0.5-m meshes in the later processing step, as well as 31 cherry trees other than *C. jamasakura*, and we used 288 individual trees in the following analyses (35 in Shimosenbon, 163 in Nakasenbon, 60 in Kamisenbon, and 30 in Okusenbon). The means and standard deviations for height and diameter at breast height (dbh) in the selected 288 individuals were 11.4 m ± 2.8 m and 36.8 cm ± 16.7 cm, respectively. The means and standard deviations for height and dbh in the excluded five small individuals were 5.7 m ± 0.9 m and 8.9 cm ± 3.5 cm, respectively.

Among the 288 *C. jamasakura* trees, we took hemispherical photographs of 96 individuals (15 in Shimosenbon, 40 in Nakasenbon, 27 in Kamisenbon, and 14 in Okusenbon) and calculated the individual-level crown porosities. The trees with relatively upright stems and evenly distributed branches around the trunks were selected to minimize noises when comparing the field and the LiDAR data. Because the hemispherical photograph taken under the crown includes the trunk considerably, we took two photographs on opposite sides of the trunk for each tree and integrated each half not blocked by the trunk in the

following analyses (Figure 2). The photographs were taken using a fish-eye lens (Sigma Circular Fisheye 4.5-mm F2.8 EX DC) attached to a digital camera (Canon EOS 60D), which was leveled on a tripod 1.3 m above the ground, under overcast sky conditions or immediately after sunset in August 2011.

LiDAR Data
The airborne LiDAR data were collected over the study area using a RIEGL LMS-Q560 sensor (Riegl Laser Measurement Systems GmbH, Horn, Austria) mounted on a helicopter platform on August 4, 2011, which was during the leaf-on season. This system projects near-infrared laser beams (1,550 nm) and records the full waveform of the reflection. The pulse frequency was 240 kHz and the scanning angle was ±30°. The flying height was 300 m above ground-level and the beam divergence was 0.5 mrad, thereby yielding a ground footprint measuring approximately 0.15 m in diameter. The flight speed was around 80 km/h^{-1}. A back-and-forth flight pattern was used to survey the entire area. The full-waveform data from the entire area were converted into discrete points by detecting the local amplitude maxima of the

Table 1. Tree health indicators used for visual rank assessment (Shibata 2007).

| Indicators	Abbreviation	Rank 1	Rank 2	Rank 3	Rank 4
Tree vigor	Tvg	vigorous growth	slight decline in vigor (not conspicuous)	clear decline in vigor	clearly poor growth state and no prospect of recovery
Tree form	Tfm	maintenance of the natural tree form	slight loss of the natural tree form (not conspicuous)	conspicuous loss of the natural tree form	complete loss of the natural tree form
Branch growth	Bgr	normal (≥ 30 cm at the top)	slightly less than rank 1	new branches are short and thin	new branches are extremely short
Crown dieback	Cdb	no dieback	slight dieback (not conspicuous)	conspicuous dieback or cuttings	severe dieback or cutting
Crown density	Crd	closed crown and high density of branches and leaves	slightly less than rank 1	distinct porosity with sparse branches and leaves	many dead branches, poor leaf development, and very sparse crown
Leaf shape and size	Lsh	normal	few deformed or small leaves	deformed leaves or generally small leaves	many deformed leaves or conspicuously small leaves
Leaf color	Lcl	normal	few pale leaves or diseased leaves	abnormal (many pale leaves or diseased leaves)	conspicuously abnormal leaves
Bark condition	Brk	active thickening growth and active bark regeneration	normal	old bark, no bark regeneration, or damage	very old bark, distinct damage, or decay
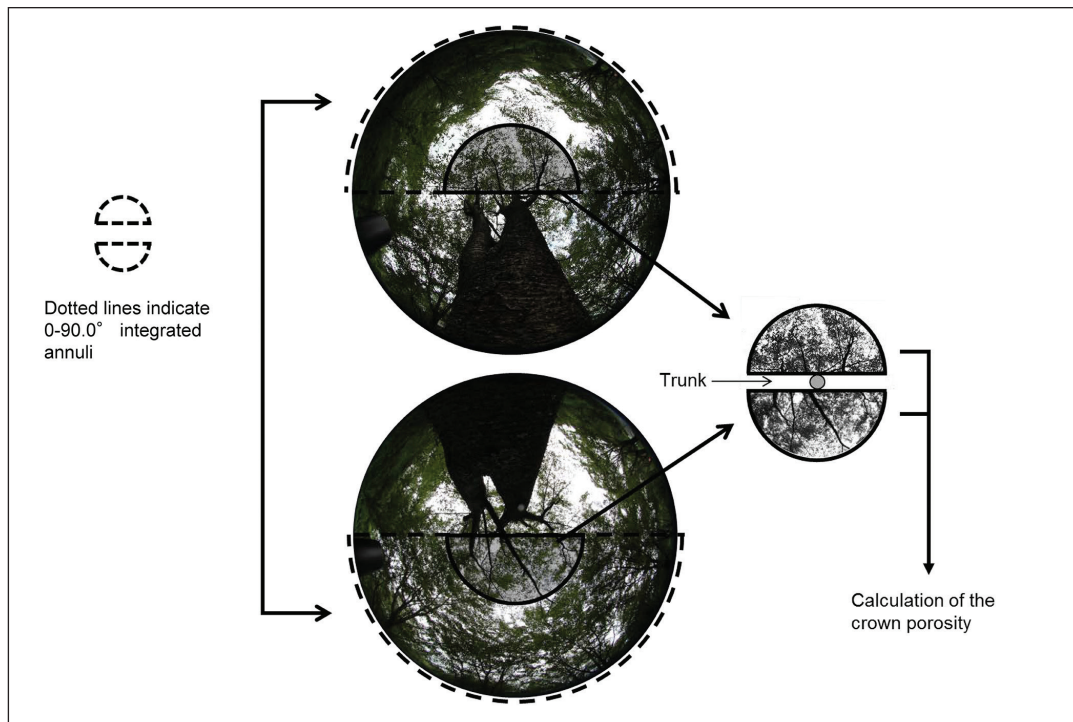
Figure 2. Calculation of the individual-level crown porosity based on a hemispherical photograph. The two hemicycles framed by the solid lines were integrated and the porosity was calculated.

waveforms (by Nakanihon Air Service Co. Ltd., Japan). All of the points obtained had x-, y-, and z-coordinate values and any of following attributes: *first*, *intermediate*, *last*, or *only* returns. *First*, *intermediate*, and *last* refer to the order in which the projected laser hit the tree components while passing through the crown. If all of the energy from a projected laser was returned at the same time, it was recorded as an *only* return.

Data Processing

Calculation of Crown Porosity
The individual-level crown porosity was calculated based on the hemispherical photographs of each of the 96 trees using CanopOn 2 software (Takenaka 2009), which binarized all the pixels in a hemispherical photograph to classify them as either sky or vegetation, where the hemispherical photograph was divided into 11 annulus rings split at zenith angles of 8.6°, 16.0°, 24.3°, 32.4°, 40.9°, 49.9°, 57.8°, 65.0°, 73.2°, 81.7°, and 90.0°. Thus, 11 gap fraction values were calculated according to the integrated annuli from 0–8.6° to 0–90.0°. For each of the two

photographs per tree, we selected the zenith angle to completely cover the crown on the opposite side from the trunk (Figure 2), with the exception of abnormally long branches and overlaps with adjacent trees. The porosity value was calculated by integrating two hemicycles per tree, which we defined as the *crown porosity*.

LiDAR Data Processing
A 0.5-m mesh digital elevation model (DEM) was created by building a triangulated irregular network according to the public manual (Geospatial Information Authority of Japan 2006). For all the LiDAR points, we derived their height above the ground using the DEM data, and the points with height ≥ 1.3 m were classified as "vegetation" points and the remaining as "ground" points. The numbers of the "vegetation" points and "ground" points were exported with 0.5-m meshes. The numbers of the points with each return type, i.e., first, intermediate, last, and only returns, were also exported with 0.5-m meshes.

The numbers of points in each class and each return type within each crown polygon were calculated. The meshes on the polygon border line were

dealt with as the meshes in the polygon if the center of the mesh was included in the polygon. Thus, the mean and standard deviation of the point density inside the crown were 167.0 and 81.4 points/m² or m⁻², respectively ($n = 288$). We calculated ten LiDAR variables based on previous studies (Morsdorf et al. 2006; Sasaki et al. 2008; Korhonen et al. 2011; Sasaki et al. 2016b) for each tree crown (Table 2), all of which represented the proportion of laser hits within the crowns using the information obtained from the point classes (vegetation or ground) and attributes (first, intermediate, last, or only).

Ordination and Correlation Analysis

For the 288 *C. jamasakura* trees, each 4-rank health indicator (Table 1) was converted into binary value: for example, if the "Tree vigor (Tvg)" for a tree is rank 3, the rank value is expressed by four binary values; Tvg1: 0, Tvg2: 0, Tvg3: 1, Tvg4: 0. This conversion was conducted for the data of the two experts respectively. Using the produced binary data, detrended correspondence analysis (DCA) was conducted using the vegan package in R version 3.4.1. (R Development Core Team). DCA is an improved method of correspondence analysis (CA) and corrects "arch effect" inherent to CA when using unimodal data (Hill and Gauch 1980). By this method, the health indicators for each rank were ordinated along the axes. The scores of the first axis by the two experts were averaged for each tree and used in the following analyses (hereinafter, referred to as "DCA axis 1 score"). Relationships between the DCA axis 1 score and the ten LiDAR variables (Table 2) were investigated using Pearson's correlation coefficient.

For the 96 individuals with hemispherical photographs, relationships between the crown porosities in the photographs and the ten LiDAR variables were assessed using Pearson's correlation coefficients. Correlation between the DCA axis 1 score and the crown porosity was also calculated.

Estimating the Tree Health Condition and Crown Porosity Using LiDAR Variables

We verified whether the DCA axis 1 score could be estimated using the LiDAR variables. A generalized linear model (GLM) was produced using a Gaussian distribution as an error distribution. To eliminate multicollinearity, if the correlation coefficients among the explanatory variables exceeded 0.5, that with a lower correlation with the response variable was eliminated in order. The conceivable regression models were arranged in the ascending order of Akaike's information criterion (AIC), and the model with the lowest AIC was selected as the best model. The effectiveness of the models was verified using the root mean squared error (RMSE) and the Pearson's correlation between the estimated values and the measured values.

Table 2. LiDAR indices used in the present study.

Abbreviation	Calculation Method	Reference
V_{ALL}	$N_{Vegetation}/N_{All}$	Maltamo et al. 2004; Sasaki et al. 2008; 2016b
V_{FO}	$N_{Vegetation}/(N_{First} + N_{Only})$	Sasaki et al. 2008
VF_{FO}	$N_{VegetationFirst}/(N_{First} + N_{Only})$	Sasaki et al. 2016b
VL_{LO}	$NV_{egetationLast}/(N_{Last} + N_{Only})$	Sasaki et al. 2016b
VO_{FO}	$N_{VegetationOnly}/(N_{First} + N_{Only})$	
$VFVO_{FO}$	$(N_{VegetationFirst} + N_{VegetationOnly})/(N_{First} + N_{Only})$	Korhonen et al. 2011
$VLVO_{LO}$	$(N_{VegetationLast} + N_{VegetationOnly})/(N_{Last} + N_{Only})$	Korhonen et al. 2011
VO_{ALL}	$N_{VegetationOnly}/N_{All}$	
VO_O	$N_{VegetationOnly}/N_{Only}$	Sasaki et al. 2008
VO_{VFVO}	$N_{VegetationOnly}/(N_{VegetationFirst} + N_{VegetationOnly})$	Sasaki et al. 2016b

N_{All}	Number of all the returns
N_{First}	Number of the "first" returns
N_{Last}	Number of the "last" returns
N_{Only}	Number of the "only" returns
$N_{Vegetation}$	Number of the vegetation returns
$N_{VegetationFirst}$	Number of the "first" returns within the vegetation returns
$N_{VegetationLast}$	Number of the "last" returns within the vegetation returns
$N_{VegetationOnly}$	Number of the "only" returns within the vegetation returns

The crown porosity in the hemispherical photographs was also estimated by the GLM using the LiDAR variables. The binomial distribution and logit were used as an error distribution and a link function, respectively. The relationships between the estimated and measured values were verified using Pearson's correlation coefficient.

We analyzed influences of tree size on estimation accuracies by comparing the crown areas with the differences between estimated and measured values.

RESULTS

Results of Field Survey and Ordination
The result of DCA ordination was shown in Figure 3. All of the health indicators were arranged from 1 (good) to 4 (poor) in the ascending order of the DCA axis 1 score.

The median, maximum, and minimum values of the DCA axis 1 score for the trees were −0.12, 3.03, and −1.70, respectively (Figure 4). For the crown porosity values obtained from the hemispherical photographs, the median, maximum, and minimum values were 0.174, 0.533, and 0.082, respectively (Figure 4).

Correlation Analyses
The correlation between the DCA axis 1 score and the crown porosity was 0.704 ($p < 0.001$). Table 3 shows the correlations of the LiDAR variables with DCA axis 1 score and with crown porosity. Many of the LiDAR variables had significant coefficients with each variable. VO_{VFVO} had the strongest correlations with both DCA axis 1 score and crown porosity (–0.600 and –0.617, respectively; $p < 0.001$).

Estimating Health Condition and Crown Porosity Using LiDAR Variables
Table 4 shows selected explanatory variables and the results obtained by the GLM. VO_{VFVO} and V_{FO} were selected to estimate the DCA axis 1 score. We only used VO_{VFVO} for the GLM because it had the lowest AIC value. The RMSE value was 0.803, and the correlation coefficients between the estimated and measured values was 0.600 ($p < 0.001$).

VO_{VFVO} and VL_{LO} were selected to estimate the crown porosity. We only used VO_{VFVO} for the GLM because it had the lowest AIC value. The RMSE value was 0.060 and the correlation coefficient between the estimated and measured values was 0.643 ($p < 0.001$).
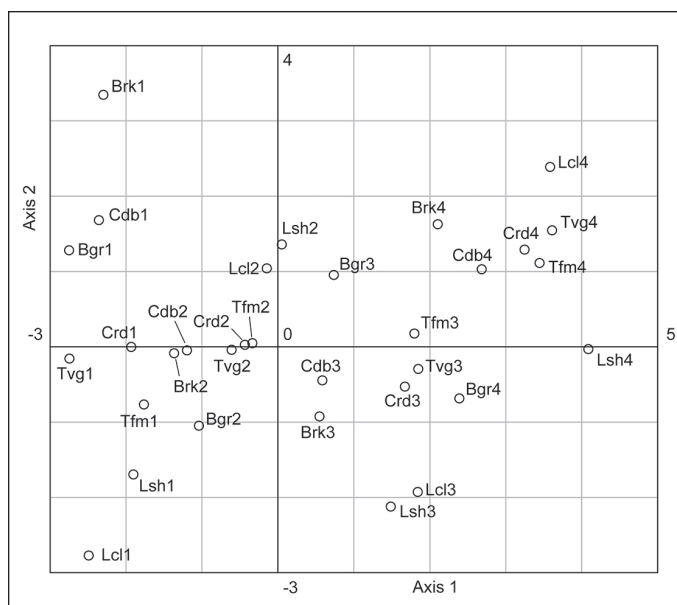

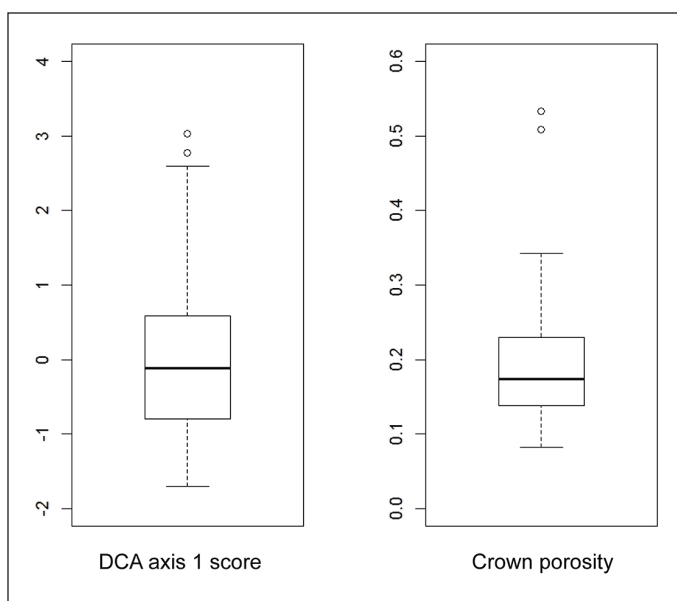Figure 3. DCA results for 4-rank assessment items.

Figure 4. Ranges of DCA axis 1 scores (*n* = 288, means of the values given by the two experts) and crown porosity determined from hemispherical photograph (*n* = 96).

Relationships Between the Estimation Accuracy and Crown Area
We analyzed whether the difference between estimated and measured values of the DCA axis 1 score and the crown porosity were influenced by the crown area (Figure 5). The individuals with larger crowns tended

Table 3. Correlations between the LiDAR indices and DCA axis 1 scores ($n = 288$) and crown porosity from hemispherical photographs ($n = 96$).

	DCA axis 1 score		Crown porosity	
V_{ALL}	−0.390	**	−0.459	**
V_{FO}	0.075		0.001	
VF_{FO}	0.510	**	0.456	**
VL_{LO}	−0.048		−0.192	
VO_{FO}	−0.578	**	−0.615	**
$VFVO_{FO}$	−0.262	**	−0.360	*
$VLVO_{LO}$	−0.495	**	−0.579	**
VO_{ALL}	−0.459	**	−0.581	**
VO_O	−0.574	**	−0.552	**
VO_{VFVO}	−0.600	**	−0.617	**

Pearson's correlation coefficient was used.

*: $p < 0.01$; **: $p < 0.001$

to have smaller errors. For the DCA axis 1 score, the individuals with crown areas larger than 100 m² had errors smaller than 1. For the crown porosity, this tendency was similar, but one individual with a crown area of 90.3 m² had by far the largest error (0.265). This tree, which had the largest crown porosity, was the outlier of the data (0.533, Figure 4). Another outlier individual with the second largest crown porosity (0.509, Figure 4) had the second largest error (0.187, Figure 5).

DISCUSSION

Possibility of Using Crown Density/ Porosity to Estimate Tree Health

The DCA result indicated that all the health indicators showed similar arrangement along axis 1 (Figure 3), thereby suggesting that estimating some health indicators with high accuracy could facilitate the estimation of the total tree health condition. In addition, the DCA axis 1 score appeared to indicate the total health condition of the trees. The correlation coefficient between the DCA axis 1 score and the crown porosity was high ($r = 0.704$, $p < 0.001$), indicating objectivity of the traditional visual assessment made by experts. This result suggested that it is possible to estimate the total health condition by estimating the crown density/ porosity using LiDAR data.

Relationships Between LiDAR Variables and Indicators Obtained in the Field

Of the LiDAR variables, VO_{VFVO}, representing the ratio of "only" returns among the "vegetation" returns, had the strongest negative correlations with both the DCA axis 1 score and crown porosity (Table 3). It was presumed because healthy trees have closed crowns, thereby increasing the likelihood of lasers being reflected from the crown surfaces. According to a previous study, VO_{VFVO} was effective for estimating the canopy porosity in a forest with simple structure, similar-aged trees, less canopy surface roughness, and few understory trees (Sasaki et al. 2016b). In this study site, only cherry trees have been planted, and there are very few other trees and shrubs under the crowns of the cherry trees, resulting in a simple woodland structure. In addition, we did not need to consider the gaps between tree crowns and the differences of forms and heights among adjacent trees because we calculated the porosity within the crown at the individual tree level. These conditions seemed to lead to results similar to a forest with a simple structure.

Table 4. The explanatory variables selected and the results of GLM (DCA axis 1 value: $n = 288$; crown porosity from hemispherical photographs: $n = 96$).

Response variables	Order	Regression coefficients				AIC	RMSE	Pearson's correlation coefficients between estimated and measured values
		Intercept	V_{FO}	VL_{LO}	VO_{VFVO}			
DCA axis 1 score	1	1.443			−3.804	696.66	0.803	$r = 0.600$ ($p < 0.001$)
	2	1.916	−0.307		−3.904	696.68		
	3	−0.477	0.337			823.82		
Crown porosity	1	−0.618			−2.128	48.53	0.060	$r = 0.643$ ($p < 0.001$)
	2	−1.254		−0.775		50.08		
	3	−0.435	−0.743		−2.126	50.19		

On the other hand, V_{ALL}, the complement of which has been verified as an effective variable for estimating the leaf area and canopy porosity in various types of forests (Riaño et al. 2004; Sasaki et al. 2008; Richardson et al. 2009; Sasaki et al. 2016b), had smaller correlation coefficients than VO_{VFVO} with both of the two variables (Table 3), although they were significant. V_{ALL} counts all the points that hit the forest vegetation components above 1.3 m, including the sub-canopy and shrub layers, so it will increase the stability when measuring complex structures in forests (Sasaki et al. 2016b). However, in this study, it was hardly necessary to consider the vegetation components under the crown, which appeared to increase the noise caused by the lasers hitting the trunk.

GLM Results and Estimation Accuracy

The GLM estimates of the DCA axis 1 score and the crown porosity demonstrated the effectiveness of VO_{VFVO} because for both of the two variables, the AIC values were the lowest, and there were significant correlations between the estimated and measured values when using only VO_{VFVO} as an explanatory variable (Table 4).

According to the estimate of the DCA axis 1 score, the individuals with large crown areas (> 100 m^2) had small errors (< 1) between the estimated and measured values (Figure 5). For the crown porosity, this tendency was similar except for the outlier individuals (Figure 5). In previous LiDAR studies, small trees were more difficult to measure compared to large trees when monitoring forest canopies (Zimble et al. 2003; Maltamo et al. 2004). The results of the present study are consistent with those of previous studies, thereby suggesting that airborne LiDAR is effective for individual tree health estimation, but a large crown size is necessary to obtain more accurate estimates.

CONCLUSION

The results of this study suggest that the total tree health condition can be estimated by the crown density or porosity because the DCA axis 1 score from the visually assessed health indicators had a strong correlation with the crown porosity determined from hemispherical photographs. Furthermore, the LiDAR variables had significant relationships with the tree health indicator; in particular, VO_{VFVO}, which represents the proportion of the lasers reflected from the crown surface, seemed to be the most effective. These
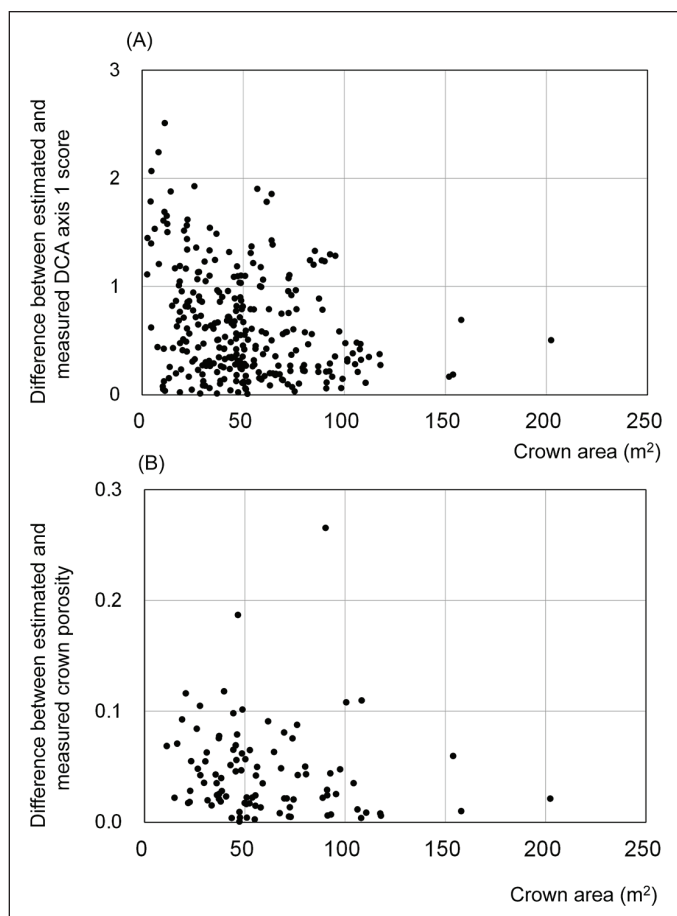

Figure 5. The relationships between crown area of the trees and difference between estimated and measured (A) DCA axis 1 score and (B) crown porosity.

results may be applied to monitoring trees at the individual level, including trees other than *C. jamasakura*, because the LiDAR variables used in this study represent physical characteristics. This method has challenges if applied to densely forested areas with complex structures where individual tree delineation is difficult, but it will be acceptable for the diagnosis of trees in urban areas, such as parks or roadsides.

LITERATURE CITED

Chen, J.M., and J. Cihlar. 1996. Retrieving leaf area index of boreal conifer forests using Landsat TM images. Remote sensing of Environment 55: 153–162.

Ferretti, M. 1997. Forest health assessment and monitoring—issues for consideration. Environmental monitoring and assessment 48: 45–72.

Geospatial Information Authority of Japan. 2006. Digital elevation model (DEM) creating manual from airborne laser data (draft). Geospatial Information Authority A1, No. 310. Accessed 03/10/2017. <http://psgsv2.gsi.go.jp/koukyou/download/re-za/310kouku.pdf> (in Japanese).

Griffith, K.T., A.G. Ponette-González, L.M. Curran, and K.C. Weathers. 2015. Assessing the influence of topography and canopy structure on Douglas fir throughfall with LiDAR and empirical data in the Santa Cruz mountains, USA. Environmental Monitoring and Assessment 187: 1–13.

Hasegawa, S., M. Tabata, T. Kozawa, and Y. Sato. 1984. Relationship between physicality of soil and tree vigour in planting area marked by heavy construction machine. An example of high way planting area. Journal of the Japanese Institute of Landscape Architects 48: 104–122 (In Japanese with English abstract).

Hill, M.O., and H.G. Gauch. 1980. Detrended correspondence analysis: an improved ordination technique. pp. 47–58. In: Maarel, E. van der (Ed.). Classification and ordination. Springer, Dordrecht, Netherlands.

Holmgren, J., Å. Persson, and U. Söderman. 2008. Species identification of individual trees by combining high resolution LiDAR data with multispectral images. International Journal of Remote Sensing 29: 1537–1552.

Hopkinson, C. and L. Chasmer. 2009. Testing LiDAR models of fractional cover across multiple forest ecozones. Remote Sensing of Environment 113: 275–288.

Iida, Y., J. Imanishi, and Y. Morimoto. 2013. Variation distribution of budburst phenology of Japanese mountain cherry (*Cerasus jamasakura* [Siebold ex Koidz.] H. Ohba var. *jamasakura*) and its applicability. Journal of the Japanese Society of Revegetation Technology 39: 98–102 (In Japanese with English abstract).

Imanishi, J., H. Kim, Y. Iida, H. Okugawa, Y. Morimoto, K. Yamanaka, and T. Kojima. 2012. Effect of sunlight condition determined by terrain on tree health of Japanese mountain cherry (*Cerasus jamasakura* [Siebold ex Koidz.] H. Ohba var. *jamasakura*) in Yoshinoyama, Nara Prefecture, Japan. Journal of the Japanese Society of Revegetation Technology 38: 15–20 (In Japanese with English abstract).

Imanishi, J., H. Okugawa, K. Hyunjun, Y. Iida, Y. Morimoto, K. Yamanaka, and T. Kojima. 2011. Tree health assessment of *Cerasus* species during the flowering season: a case study of Japanese mountain cherry (*Cerasus jamasakura* [Siebold ex Koidz.] H. Ohba var. *jamasakura*) in Yoshinoyama, Nara Prefecture, Japan. Journal of the Japanese Society of Revegetation Technology 37: 9–14 (In Japanese with English abstract).

Imanishi, J., Y. Song, T. Sasaki, Y. Iida, Y. Morimoto, and T. Kojima. 2016. Large-scale survey of flowering cherry trees using airborne LiDAR. Proceedings of Archi–Cultural Interactions through the Silk Road 4th International Conference, 149–152.

Korhonen, L., I. Korpela, J. Heiskanen, and M. Maltamo. 2011. Airborne discrete-return LiDAR data in the estimation of vertical canopy cover, angular canopy closure and leaf area index. Remote Sensing of Environment 115: 1065–1080.

Kozawa, T., and T. Kobayashi. 1998. The objective evaluation method of the tree vigor with the stem temperature.—The development of a plant vigor measuring instrument—. Journal of Japan Society of Civil Engineers. 622: 81–86 (In Japanese with English abstract).

Lefsky, M.A., W.B. Cohen, G.G. Parker, and D.J. Harding. 2002. LiDAR remote sensing for ecosystem studies. BioScience 52: 19–30.

Lim, K., P. Treitz, M. Wulder, B. St-Onge, and M. Flood. 2003. LiDAR remote sensing of forest structure. Progress in Physical Geography 27: 88–106.

Long, R. P., S.B. Horsley, and P.R. Lilja. 1997. Impact of forest liming on growth and crown vigor of sugar maple and associated hardwoods. Canadian Journal of Forest Research 27: 1560–1573.

Maltamo, M., K. Eerikäinen, J. Pitkänen, J. Hyyppä, and M. Vehmas. 2004. Estimation of timber volume and stem density based on scanning laser altimetry and expected tree size distribution functions. Remote Sensing of Environment 90: 319–330.

Michez, A., H. Piégay, J. Lisein, H. Claessens, and P. Lejeune. 2016. Classification of riparian forest species and health condition using multi-temporal and hyperspatial imagery from unmanned aerial system. Environmental Monitoring and Assessment 188: 1–19.

Mizoue, N., and M. Dobbertin. 2003. Detecting differences in crown transparency assessments between countries using the image analysis system CROCO. Environmental Monitoring and Assessment 89: 179–195.

Morsdorf, F., B. Kötz, E. Meier, K.I. Itten, and B. Allgöwer. 2006. Estimation of LAI and fractional cover from small footprint airborne laser scanning data based on gap fraction. Remote Sensing of Environment 104: 50–61.

Nakajima, H., A. Kume, M. Ishida, T. Ohmiya, and N. Mizoue. 2011. Evaluation of estimates of crown condition in forest monitoring: comparison between visual estimation and automated crown image analysis. Annals of Forest Science 68: 1333–1340.

Nielsen, A.B., J. Östberg, and T. Delshammar. 2014. Review of urban tree inventory methods used to collect data at single-tree level. Arboriculture & Urban Forestry 40: 96–111.

Ørka, H.O., E. Næsset, and O.M. Bollandsås. 2009. Classifying species of individual trees by intensity and structure features derived from airborne laser scanner data. Remote Sensing of Environment 113: 1163–1174.

Pontius, J. and R. Hallett. 2014. Comprehensive methods for earlier detection and monitoring of forest decline. Forest Science 60: 1156–1163.

Popescu, S.C., R.H. Wynne, and R.F. Nelson. 2003. Measuring individual tree crown diameter with lidar and assessing its influence on estimating forest volume and biomass. Canadian Journal of Remote Sensing 29: 564–577.

R Development Core Team. 2005. R: A language and environment for statistical computing. R Foundation for Statistical Computing, Vienna. ISBN3-900051-07-0, URL http://www.R-project.org

Riaño, D., F. Valladares, S. Condés, and E. Chuvieco. 2004. Estimation of leaf area index and covered ground from airborne laser scanner (Lidar) in two contrasting forests. Agricultural and Forest Meteorology 124: 269–275.

Richardson, J.J., L.M. Moskal, and S.H. Kim. 2009. Modeling approaches to estimate effective leaf area index from aerial discrete-return LIDAR. Agricultural and Forest Meteorology 149: 1152–1160.

Sasaki, T., J. Imanishi, K. Ioki, Y. Morimoto, and K. Kitada. 2008. Estimation of leaf area index and canopy openness in broad-leaved forest using an airborne laser scanner in

comparison with high-resolution near-infrared digital photography. Landscape and Ecological Engineering 4: 47–55.

Sasaki, T., J. Imanishi, W. Fukui, and Y. Morimoto. 2016a. Fine-scale characterization of bird habitat using airborne LiDAR in an urban park in Japan. Urban Forestry & Urban Greening 17: 16–22.

Sasaki, T., J. Imanishi, K. Ioki, Y. Song, and Y. Morimoto. 2016b. Estimation of leaf area index and gap fraction in two broad-leaved forests by using small-footprint airborne LiDAR. Landscape and Ecological Engineering 12: 117–127.

Schaberg, P.G., J.W. Tilley, G.J. Hawley, D.H. DeHayes, and S.W. Bailey. 2006. Associations of calcium and aluminum with the growth and health of sugar maple trees in Vermont. Forest Ecology and Management 223: 159–169.

Schnell, S., C. Kleinn, and G. Ståhl. 2015. Monitoring trees outside forests: a review. Environmental Monitoring and Assessment 187. doi: 10.1007/s10661-015-4817-7

Schomaker, M.E., S.J. Zarnoch, W.A. Bechtold, D.J. Latelle, W.G. Burkman, and S.M. Cox. 2007. Crown-condition classification: a guide to data collection and analysis. General Technical Report SRS-102. USDA Forest Service Southern Research Station, Asheville, North Carolina, U.S.

Scowcroft, P. G., J.B. Friday, T. Idol, N. Dudley, J. Haraguchi, and D. Meason. 2007. Growth response of Acacia koa trees to thinning, grass control, and phosphorus fertilization in a secondary forest in Hawai'i. Forest Ecology and Management 239: 69–80.

Shibata, S. 2007. Revegetation Technology. pp. 123–135. In: Y. Morimoto and Y. Shirahata (Eds.). Environmental Design: Conservation and Creation of the Landscapes. Asakura Publishing, Tokyo, Japan (in Japanese).

Takenaka, A. 2009. CanopOn2 hemispherical photograph analysis program. Accessed 09/18/2016. <http://takenaka-akio.org/etc/canopon2/>

Wulder, M.A., C.W. Bater, N.C. Coops, T. Hilker, and J.C. White. 2008. The role of LiDAR in sustainable forest management. The Forestry Chronicle 84: 807–826.

Zimble, D.A., D.L. Evans, G.C. Carlson, R.C. Parker, S.C. Grado, and P.D. Gerard. 2003. Characterizing vertical forest structure using small-footprint airborne LiDAR. Remote Sensing of Environment 87: 171–182.

Takeshi Sasaki (corresponding author)
Tokushima University—Graduate School of Technology, Industrial and Social Sciences
Tokushima, Tokushima
Japan

Junichi Imanishi
Kyoto University—Graduate School of Global Environment Studies
Kyoto, Kyoto
Japan

Yoshihiko Iida
United Nations University—Institute for the Advanced Study of Sustainability
Tokyo, Tokyo
Japan

Youngkeun Song
Seoul National University—Graduate School of Environmental Studies
Seoul
Korea (the Republic of)

Yukihiro Morimoto
Kyoto Gakuen University—Faculty of Bioenvironmental Science
Kameoka, Kyoto
Japan

Tamao Kojima
Sun Act Co. Ltd.
Kyoto, Kyoto

Résumé. Cette recherche examine l'utilité des données de détection et télémétrie par la lumière (LiDAR) afin d'établir la condition de santé du cerisier de montagne japonais (*Cerasus jamasakura*) à Yoshinoyama, dans la préfecture de Nara au Japon. Les variables LiDAR, qui représentent le rapport des lasers atteignant les constituantes des arbres furent calculées et leur efficacité relative fut analysée en lien avec les résultats d'évaluations conventionnelles de terrain des critères visuels de santé des arbres en fonction d'ordonnancement, d'analyses corrélatives et de modèles linéaires généralisés. Les résultats montrèrent que plusieurs variables LiDAR avaient des corrélations significatives avec les variables découlant de l'observation visuelle de la condition de santé des arbres. Particulièrement la proportion des seuls retours, qui représentent le rapport des lasers réfléchis par la surface du houppier, était la plus efficace pour l'appréciation de la condition globale de santé en lien avec la densité du houppier, un des indicateurs-clefs de santé représentant les propriétés physiques. Les arbres montrant d'importantes erreurs d'évaluation possédaient de plus petits houppiers que les arbres avec peu d'erreurs, suggérant que les dimensions suffisamment imposantes de houppiers étaient importantes afin d'obtenir des évaluations précises pour l'utilisation de données LiDAR en vue de l'établissement de la condition de santé.

Zusammenfassung. Diese Studie untersucht die Nützlichkeit von Daten aus einer optischen Abstands- und Geschwindigkeitsmessung von Licht (LIDAR) für die Einschätzung individueller Baumgesundheitskonditionen von japanischen Zierkirschen (*Cerasus jamasakura*) in Yoshinoyama, Präfektur Nara, Japan. Die LIDAR-Variablen, welche das Verhältnis von Laserstrahlen, die auf die Baumbestandteile treffen, werden kalkuliert und ihre Effektivität wird dadurch gemessen, dass sie mit den Ergebnissen konventioneller, visueller Baumkontrollen vorort basierend auf Ordination, Korrelationsanalysen und generalisierten linearen Modellen in Relation gesetzt werden. Die Ergebnisse zeigen, dass viele der LIDAR-Variablen signifikante Korrelationen mit den Variablen aus der visuellen Baumkontrolle aufwiesen. Besonders die Proportion von „nur"-Rückmeldungen, welche das Verhältnis der reflektierten Laserstrahlen aus der Kronenoberfläche repräsentieren, waren sehr effektiv, um den absoluten Gesundheitszustand in Relation zur Kronendichte zu schätzen, einer der Schlüsselindikatoren für die physikalischen Gegebenheiten. Die Individuen mit großen Schätzungsfehlern hatten schmalere Kronen als die Individuen mit kleinen Fehlern, was darauf hindeutet, dass ausreichend große Kronengrößen wichtig sind für

präzisere Schätzungen der Baumgesundheit, wenn die Daten aus der LIDAR-Messung verwendet werden.

Resumen. Este estudio examinó la utilidad de los datos de detección y alcance de la luz aerotransportada (LiDAR) para estimar la condición de salud de árboles de cereza de montaña japonesa (*Cerasus jamasakura)* en Yoshinoyama, Prefectura de Nara, Japón. Se calcularon las variables LiDAR que representaban la proporción de los láseres que golpeaban las partes del árbol y se examinó su efectividad relacionándolas con los resultados de las evaluaciones visuales de salud de los árboles obtenidos en el campo mediante la ordenación, análisis de correlación y modelos lineales generalizados. Los resultados mostraron que muchas de las variables LiDAR tenían correlaciones significativas con la variable derivada de la condición de salud del árbol evaluada visualmente. En particular, la proporción de "únicamente" retornos, lo cual representa la relación de los láseres reflejados desde las superficies de la copa, fue la más efectiva para estimar el estado de salud total en relación con la densidad de la copa, uno de los indicadores clave de salud para representar las propiedades físicas . Los individuos con grandes errores de estimación tenían copas más pequeñas que los individuos con pequeños errores, lo que sugiere que los tamaños de copa suficientemente grandes son importantes para obtener estimaciones más precisas de la condición de salud del árbol utilizando datos de LiDAR.